Journal of
Ceramic Science
and Technology

J. Ceram. Sci. Tech., **03** [02] 81-88 (2012)
DOI: 10.4416/JCST2012-00003
available online at: http://www.ceramic-science.com

Robocasting of Alumina Lattice Truss Structures

T. Schlordt*, F. Keppner, N. Travitzky, P. Greil

Department of Materials Science, Glass and Ceramics, Friedrich-Alexander-University Erlangen-Nuernberg, Martensstr. 5, 91058 Erlangen, Germany

received January 20, 2012; received in revised form February 8, 2012; accepted February 25, 2012

Abstract

Robocasting of aqueous colloidal α-Al_2O_3 gels for manufacturing cellular ceramics with periodical lattice truss structures was investigated. Coagulation of gels loaded with 48 vol% α-Al_2O_3 was induced by adding CH_3COONH_4. The gels exhibit shear-thinning behavior, shear elastic moduli ranging from 6.7 to 390 kPa and yield-stresses from 25 to 570 Pa. Continuous filaments with a diameter of 0.5 mm were extruded with a deposition speed of up to 35 mm/s on a high-precision six-axis robotic system equipped with a single-screw micro-extruder. The lattice structures consist of alternating layers formed by a linear array of circular rods aligned parallel with a distance of 1 mm and an angle of 90° between alternating layers. After being dried for 12 h, the robocast grids were sintered in air at 1650 °C for 2 h resulting in a fractional strut density > 0.95, a mean filament diameter of 400 μm, a volume filling fraction of 0.49 (sealed walls) and 0.35 (meshed walls), and macro-cells in the deposition plane of quadratic shape with a mean area of 0.136 mm^2 ± 0.017 mm^2 Based on gravitation-driven viscous flow, model conditions for attaining free spanning ligaments were discussed.

Keywords: Robocasting, alumina gel, lattice truss structures

I. Introduction

Moldless robocasting of ceramics is a solid freeform technique working on the principle of continuous writing of a filament and layer-by-layer build-up of a three-dimensional filamentary preform [1,2]. Aqueous colloidal gels and colloid-loaded thermoplastic polymers were applied to demonstrate the capability of robocasting technology to manufacture three-dimensional preforms with excellent shape variability including high aspect walls as well as unsupported spanning structures [3]. While robocasting in air was successfully performed applying nozzles with diameters exceeding 500 μm, decoupling the deposition kinetics from the drying process by extrusion into a non-wetting oil bath allowed the generation of filament diameters smaller than 100 μm [4]. The dried extruded preform can be sintered without a separate debinding process as only a low organic content (< 3 wt%) is required. Applications include manufacturing of grid and lattice structures for composites, bone restoration and meshes for filters. Ceramic gels based on silica [1], alumina [5–7], mullite [8], lead-zirconate-titanate [9], tricalciumphosphate [10], hydroxyapatite [11], lead-magnesium-niobate (PMN) [12], porcelain [13] and barium-titanate [14] were applied to robocasting. Gelation was induced by lowering the pH-value, increasing the ionic strength or adding a polymeric flocculant. In order to prevent sedimentation and syneresis, cellulose derivatives were added which may give rise to appreciable yield-stress of the particle suspension [15]. Depending on the extrusion speed and rheological behavior, flow of a colloidal gel through the extrusion nozzle may cause a pronounced shear-rate gradient over the filament diameter. Plug-flow with an unyielded core and a surface region depleted of particles (slip-plane) was reported [4]. The opportunities and challenges of robocasting e.g. direct filament writing were surveyed in an excellent review by Lewis *et al.* [1].

In this work, a novel six-axis robot system was coupled to a single-screw micro-extruder to provide high geometrical precision and line control flexibility for continuous filament writing. Regular grids of alumina were manufactured with an aqueous-based alumina gel feedstock. The rheological behavior of the colloidal alumina gel was systematically varied by adding CH_3COONH_4 (NH_4Ac). Yield stress, shear elastic modulus and relaxation kinetics of the gel filaments were analyzed to select optimum parameters for control of shape and dimensional stability. Three-dimensional lattice truss structures of alumina were manufactured, and the potential of robot-assisted continuous filament deposition was demonstrated.

II Experimental Procedure

(1) Preparation of the colloidal alumina gel

An aqueous slurry containing 52 vol% (81 wt%) of a submicron α-Al_2O_3 powder (CT3000 SG, Almatis GmbH, Ludwigshafen, Germany, d_{50} = 0.35 μm, S_V = 8.3 m^2/g) was prepared in a tumbling mixer (Turbula T2F, Willi A. Bachofen AG, Muttenz, Switzerland) using ZrO_2 milling balls. The slurry contained 1.6 wt% NH_4-polymethacrylate dispersant (Darvan C-N, R.T. Van-

* Corresponding author: tobias.schlordt@ww.uni-erlangen.de

derbilt Co. Inc., Norwalk, USA, M_w = 1.5 x 10^4 g/mol) and 0.42 wt% (10.83 g/l) ethyl-hydroxyethyl-cellulose (Bermocoll E 320 FQ, Akzo Nobel GmbH, Dueren, Germany, M_w ~ 1.1 x 10^5 g/mol). After agitation for 72 h at 67 min^{-1}, NH_4Ac (Merck KGaA, Darmstadt, Germany) solution was added as coagulant. The gel was homogenized and degassed in a centrifugal planetary mixer (ARE-250, Thinky Corporation, Tokyo, Japan) for 6 min at 2000 min^{-1}. The pH was monitored (pH 21, HI1110 electrode, HANNA Instruments Deutschland GmbH, Kehl, Germany) and varied only slightly within the range 8.3 – 9. With increasing NH_4Ac concentration, the total ionic strength I [14] calculated from the molar concentration M_i and the valency z_i of species i (e.g. $z_{NH_4^+} = 1$ and $z_{CH_3COO^-} = -1$)

$$I = 0.5 \sum_i M_i z_i^2 \quad (1)$$

rises, and contraction of the electrosteric layer around the alumina particles gives rise to coagulation [20]. Thus, increase of the NH_4Ac concentration from 0 to 1.95 wt% (M_{NH_4Ac} = 0 – 0.649 mol/l) correlates with an increase of yield stress τ_y, shear elastic modulus G' and viscosity parameter κ, Table 1. The viscosity was measured at 20 °C with a stress-controlled rheometer (AR G2, TA Instruments, Elstree, UK) with a cleated parallel plate geometry (diameter 40 mm, gap 1 mm) [16]. A solvent trap was applied to facilitate long measuring cycles. Since filament extrusion requires the colloidal suspension to flow through the deposition nozzle at high shear stresses and shear rates, the rheological data from rotational measurements of the viscosity η were fitted to a rheological model developed for colloidal gels at high shear rates [17]

$$\eta = \eta_\infty + \kappa \left(\frac{d\gamma}{dt}\right)^{\nu - 1} \quad (2)$$

The viscosity at infinite shear, η_∞, was described by the Krieger-Dougherty Model [18]

$$\eta_\infty = \eta_s \left(1 - \frac{\phi}{\phi_m}\right)^{-[\eta]\phi_m} \quad (3)$$

η_s is the viscosity of the particle free liquid phase ($\eta_s \approx$ 0.154 Pa·s), Φ is the solids volume fraction of the alumina gel (Φ = 0.48) and Φ_m is the solids volume fraction at maximum packing (Φ_m = 0.68 [17]). Taking the intrinsic viscosity $[\eta]$ = 2.5 [18, 19], a value of $\eta_\infty \approx$ 1.82 Pa·s was derived for the colloidal alumina gel. Values of κ and ν-1 were obtained by plotting η-η_∞ versus shear rate and regression analysis of Eq. (2). The shear rate $d\gamma/dt$ was increased from 0.1 s^{-1} to 1000 s^{-1}. Stress-sweeps with gradual increase of shear stress τ from 1 Pa to 2000 Pa were performed at a frequency of 1 Hz after an oscillatory preshear at shear strain γ = 100 %. After a relaxation period of 1 h, yield-stress t_y and equilibrium shear elastic modulus G'_{equi} were determined. G'_{equi} corresponds to the plateau of the real part of the complex shear modulus G^* at low shear stresses (1 Pa to 10 Pa in this work).

(2) Robocasting

Three-dimensional alumina grids with periodical lattice structure were manufactured on a six-axis robotic system equipped with a single-screw micro-extruder (RobFab, Battenberg ROBOTIC GmbH & Co. KG, Marburg, Germany), Fig. 1. Real-time tactile and optical sensor control operating at a frequency of 200 Hz allows deposition of a continuous filament with a lateral resolution < 50 μm at a line deposition velocity of 35 mm/s. Temperature and relative humidity in the fabrication chamber (400 x 400 x 400 mm^3) were kept constant at 20 °C and 22 %, respectively. A stainless steel nozzle (Model Number 100792, UES AG, Krefeld, Germany) with a circular hole having a diameter D = 500 μm was used. The models for the alumina grid structures were designed with PyCaster, custom-designed CNC software and exported in G-code format. Three-dimensional lattice truss grids of 40 x 40 x 6.3 mm^3 with straight ligaments with a diameter D of approximately 500 μm and a cell size of 1 x 1 mm^2 were generated. The alternating distance between two deposited filaments in z-direction, d_z, was adjusted to $d_z = D$ and $d_z = D/2$, respectively.

Table 1: Rheological data of the colloidal alumina gels differing in NH_4Ac coagulant content

	NH_4Ac coagulant content						
	0	10	20	30	40	50	[g/l]
	0	0.39	0.78	1.17	1.56	1.95	[wt%]
	0	0.129	0.259	0.389	0.519	0.649	[mol/l]
pH	9	8.6	8.4	8.4	8.3	8.4	
Ionic strength I [M]	0.12	0.25	0.38	0.51	0.64	0.77	
Yield stress τ_y [Pa]	25	80	80	225	500	570	
Shear elastic modulus G'_{equi} [kPa]	6.7	75	138	191	303	389	
Viscosity parameter κ	70	187	320	711	1089	1814	
Shear thinning index ν	0.049	0.08	0.039	0.038	0	0.046	

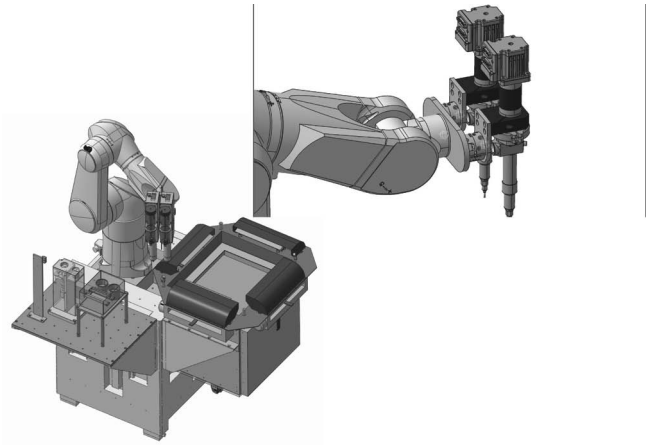

Fig. 1: Scheme of six-axis high-precision robotic system applied for robocasting (though equipped with a dual-channel deposition system only one deposition channel was applied in this work).

(3) Sintering

The robocast alumina grid samples were dried in air at relative humidity of 25 % for 12 h at 22 °C. The grids were subsequently sintered in an electrically heated furnace (HT16/17, Nabertherm GmbH, Lilienthal, Germany). A heating rate of 2 °C/minwas applied up to 450 °C to make sure the removal of organic constituents was completed. Heating rate up to 1650 °C was raised to 5 °C/min and the peak temperature was maintained for 2 h followed by cooling at a rate of 10 °C/min. Strut density of the sintered alumina struts was determined with He gas pycnometry (Accupyc 1330, Micromeritics GmbH, Moenchengladbach, Germany) from crushed specimens. The microstructure of the sintered struts and the strut crossings were analyzed with SEM (Quanta 200, FEI, Hillsboro, USA). The sintered lattice truss samples were optically scanned and analyzed with ImageJ, a Java-based open-source image analysis tool. A minimum of 1000 cells or more were measured to derive a distribution of cell sizes. Cells in the rows close to the sample surface were excluded owing to distortion caused by reversing the deposition direction. Variation of cell size served as a figure of merit variable which was used to optimize the processing parameters.

III Results and Discussion

(1) Alumina filament suspension rheology

The robocasting process involves continuous deposition of a colloidal ceramic powder suspension filament with a high solids loading in order to reduce drying-induced shrinkage and cracking. The colloidal suspension must flow through the deposition nozzle at high shear stresses and then set immediately at low shear stress to achieve shape retention [1]. As a key step, the suspension filament experiences a rapid increase in its viscosity, undergoing a sol-gel transition. Hence, filament formation and initial shape retention require careful control of the gel viscosity, yield stress, and drying kinetics [2]. Control of interparticle forces to create gel-based filament suspensions with desired viscoelastic response may be achieved by control of pH, increase of electrolyte concentration, or addition of polyelectrolyte species [8, 14]. In this work, NH_4Ac was applied to increase the ionic strength (electrolyte concentration) in order to trigger coagulation of the colloidal alumina gel [20]. While without NH_4Ac, a low yield stress of $\tau_y = 25$ Pa was measured, addition of 50 g/l NH_4Ac caused the yield stress to increase to $\tau_y = 570$ Pa, Table 1.

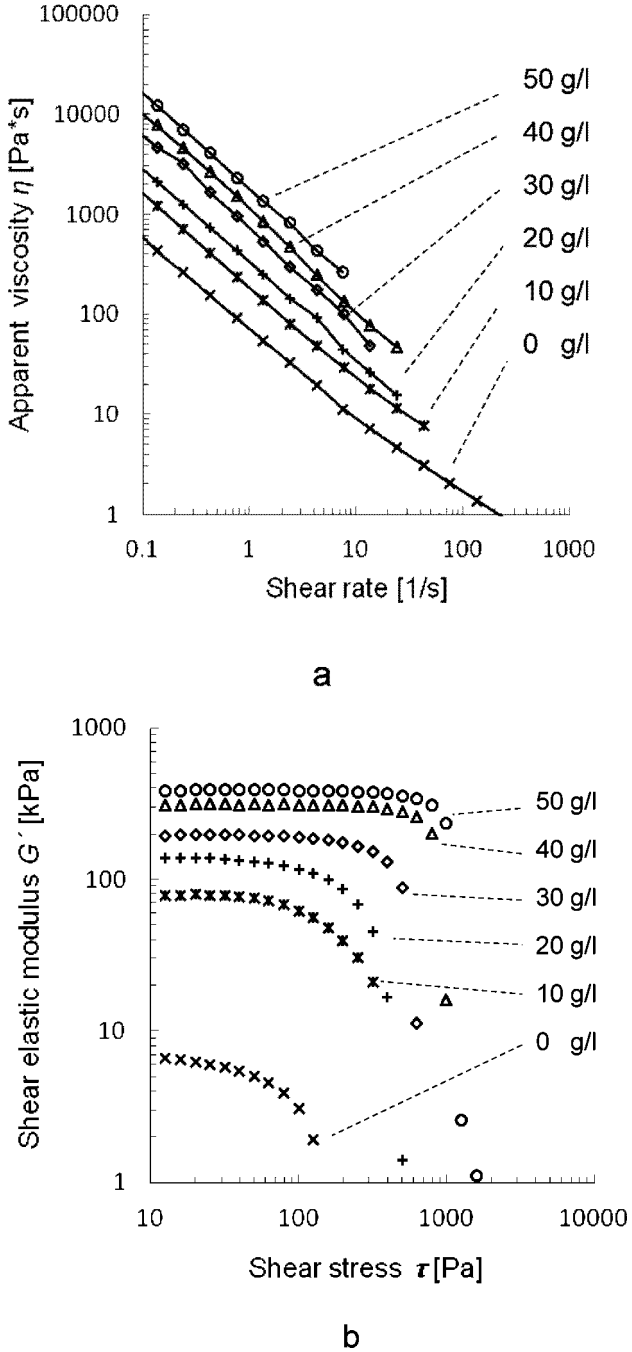

Fig. 2: Viscosity over shear rate (a) and shear elastic modulus over shear stress (b) measurements on colloidal alumina gels coagulated with different NH_4Ac concentrations.

Fig. 2 shows the results of viscosity over shear rate and shear elastic modulus over shear stress measurements. Though the reference viscosity η at 0 g/l NH_4Ac was shifted to values more than one order of magnitude higher with the addition of 50 g/l NH_4Ac, shear thinning behavior remained unaffected and the coagulated alumina gel achieved adequate rheological behavior required for the robocasting process, Fig. 2 a. Since microextrusion of the

alumina powder suspension through the submillimeter nozzle is governed by a large gradient of locally varying shear stress [17], the shear elastic modulus G' was measured at various shear stresses in stress-sweep experiments, Fig. 2 b. Without coagulant a low shear elastic modulus of $G' \leq 6.7 \times 10^3$ Pa was observed, which remained almost constant upon shear stress variation (e.g. $\equiv G'_{equi}$). Addition of NH_4Ac-coagulant resulted in a remarkable shift to $G' \sim 3.9 \times 10^5$ Pa.

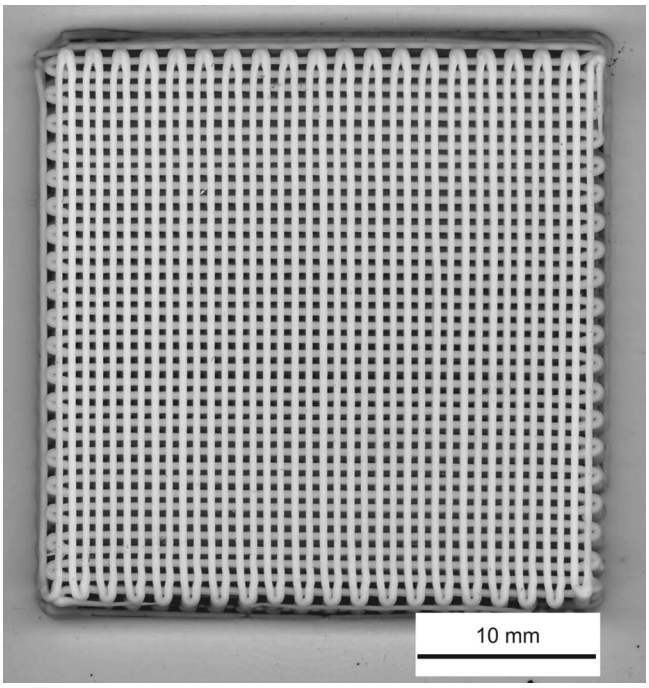

Fig. 3: Sintered alumina lattice truss structure of tetragonal cell geometry fabricated from colloidal alumina gel with a coagulant content of 50 g/l NH_4Ac applying an extrusion speed of 35 mm/s.

(2) Robocasting

Robotic deposition of a continuous filament was achieved by applying alumina gel coagulated with NH_4Ac. Fig. 3 shows a three-dimensional lattice truss structure of sintered alumina with dimensions of 32 x 32 x 3 mm^3 prepared by continuous filament writing of the alumina gel coagulated with 50 g/l NH_4Ac. The lattice structure consists of alternating layers formed by a linear array of circular rods aligned parallel with a distance of 1 mm and an angle of 90° between alternating layers. Thus, macroscopic cell patterns with tetragonal symmetry and a cell size of 1 x 1 mm^2 were formed with sealed as well as meshed walls (free-spanning ligaments). A micro-extrusion nozzle of circular geometry and a diameter of 500 μm was applied, which after sintering at 1650 °C for 2 h resulted in a filament diameter of approximately 400 μm. Optical image analysis confirms a high geometrical accuracy of the lattice geometry with the mean cell size area in the deposition plane of 0.136 $mm^2 \pm$ 0.017 mm^2. The volume filling fraction attained 0.49 (sealed walls) and 0.35 (meshed walls).

A core-shell architecture of an unyielded coagulated filament core region surrounded by a yielded fluid shell depleted in particle loading was reported to favor shape retention and fusion at the contact points [1]. Interface microstructure of the contact area after sintering of gel containing 30 g/l NH_4Ac is shown in Fig. 4. The partial penetration of the rods forming 90° junctions give an indication of joint interface formation supported by fusion. Despite a filament sintering shrinkage of ~ 20 % (radial and axial), formation of filament junctions free of visible interface defects is observed. The sintered alumina filaments are characterized by a fractional density ~ 0.95 and a uniform microstructure. No indications for radial gradient microstructure formation in the sintered filament rods were observed.

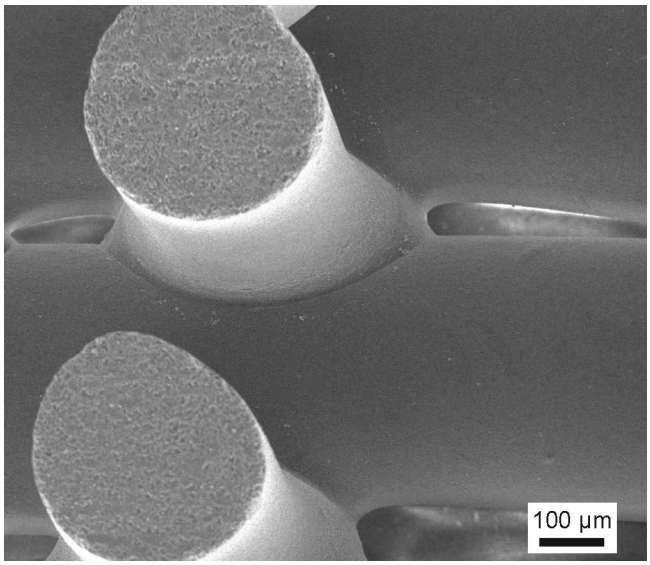

Fig. 4: Microstructure of 90° filament junctions (30 g/l NH_4Ac, 30 mm/s, 1650 °C, 2 h).

(3) Ligament deflection

Fabrication of lattice truss structures with the ligaments connected to form sealed walls as well as spanning lattice structures with free-spanning strut ligaments requires control of ligament deflection during the continuous writing process. The deposition process involves anchoring on one support, traversing of a gap with 90° bending causing tension loading, and anchoring on the second support. Fig. 5 shows the geometrical parameters considered for description of filament deflection $z(t)$ driven by gravitation during deposition of a single filament. For the case of small deflection the midspan deflection $z(t)$ at $l = l_0/2$ of a free-spanning ligament fixed between two points of distance l_0 may be expressed by

$$z(t) \approx \frac{1}{2}\sqrt{l_t(t)^2 - l_0^2} \qquad (4)$$

For the volume of the deflecting ligament to remain constant, viscous flow driven by gravitation ($d\varepsilon/dt = \sigma_n/3\eta$ with 3η resulting from Trouton's ratio [21] and $\sigma_n = \varrho g l_0/2$) causes an elongation of the ligament with time

$$l_t(t) = l_o\left(1 + \int_0^t \frac{\rho g l_o}{6\eta(t)}\,dt\right) \qquad (5)$$

where r is the density of the extruded ligament, and g is the gravitational constant. Time evolution of viscosity $\eta(t)$ is expressed by

$$\eta(t) = \eta_i + \eta_r(t) \quad (6)$$

where h_i denotes the initial viscosity while exiting the nozzle and $\eta_r(t)$ is the time-dependent recovery of viscosity of the deposited filament. The initial viscosity η_i is governed by the shear rheology profile under the geometrical constraints of the colloidal gel passing through the extrusion nozzle subjected to high shear stress [22]. Based on the Herschel-Bulkley model [23], flow through the deposition nozzle was described by adopting a three-zone velocity profile consisting of an unyielded core, surrounded by a yielded shell and possibly slip at the nozzle wall [4]. Fig. 6 a shows the steep rise of the viscosity measured after preshear of the colloidal alumina gel loaded with 30 g/l NH_4Ac. The gel was presheared at a shear rate of 100/s which corresponds to an extrusion speed of approximately 45 mm/s and subsequently subjected to a shear stress of 100 Pa (below the yield stress t_y = 225 Pa). The transition from low viscous yielded state ($\eta(t = 0) \sim 50$ Pa·s) to recovered gel state took place within less than 5 seconds ($\eta(t = 5s) \sim 4 \times 10^4$ Pa·s). Instead of calculating the unknown shear rate profile, experimental values of the time dependence of viscosity recovery $\eta(t)$ were taken to derive the deflection of a ligament with a span distance $l_0 = 1000$ μm as a function of time from Eq. (4), Fig. 6 b. The Al_2O_3 gel filament coagulated with 30 g/l NH_4Ac exhibits an instantaneous deflection of $z \approx 30$ μm within 0.3 s and approaches a constant deflection of $z \approx 40$ μm (e.g. $z/D = 0.08$) after a few seconds. Thus, assuming that a higher NH_4Ac content provides an even faster stabilization of ligament shape, formation of lattice structures with spanning distances exceeding 1 mm should be possible. Based on a static beam model, critical conditions for the minimum suspension elasticity required to avoid spanning ligament deflection were derived ($G' \geq 2.8\varrho s^4 R$) [4]. Taking values of specific weight ϱ = 2.5 g/cm^3, reduced span length $s = l_0/2R$ with beam radius R = 250 μm and unsupported beam length l_0 = 1000 μm, a minimum shear stress of $G' > 270$ kPa is derived. This value fits well to the shear elastic modulus values experimentally observed on colloidal alumina gels in the unsheared (recovered) state loaded with more than 40 g/l NH_4Ac, Fig. 2. It was concluded that the suspension must attain a higher shear elastic modulus G' when the effective suspension density, rod diameter and normalized span distance increase.

The magnitude of yield stress and the time required for the deposited filament to return fully to its gelled state after shear in the nozzle control the ability of the suspension to build unsupported spanning structures [4]. Fig. 7 shows three cases of lattice truss structures prepared by varying the gel recovery kinetics dependent on the NH_4Ac content: (a) a sealed filament wall structure is formed at a NH_4Ac content of 30 g/l and $d_z = D/2$; (b) formation of a meshed wall structure is observed at similar NH_4Ac content 30 g/l but $d_z = D$; and (c) rapid shape stabilization facilitates formation of undeflected truss structures at NH_4Ac content 50 g/l and $d_z = D$. Thus, suitable conditions for fabrication of meshed lattice truss structures by means of robocasting may be tailored by controlling the coagulation behavior of the colloidal filament suspension. Furthermore, accelerated gel state recovery after leaving the extrusion nozzle may allow even higher deposition speeds than the 35 mm/s applied.

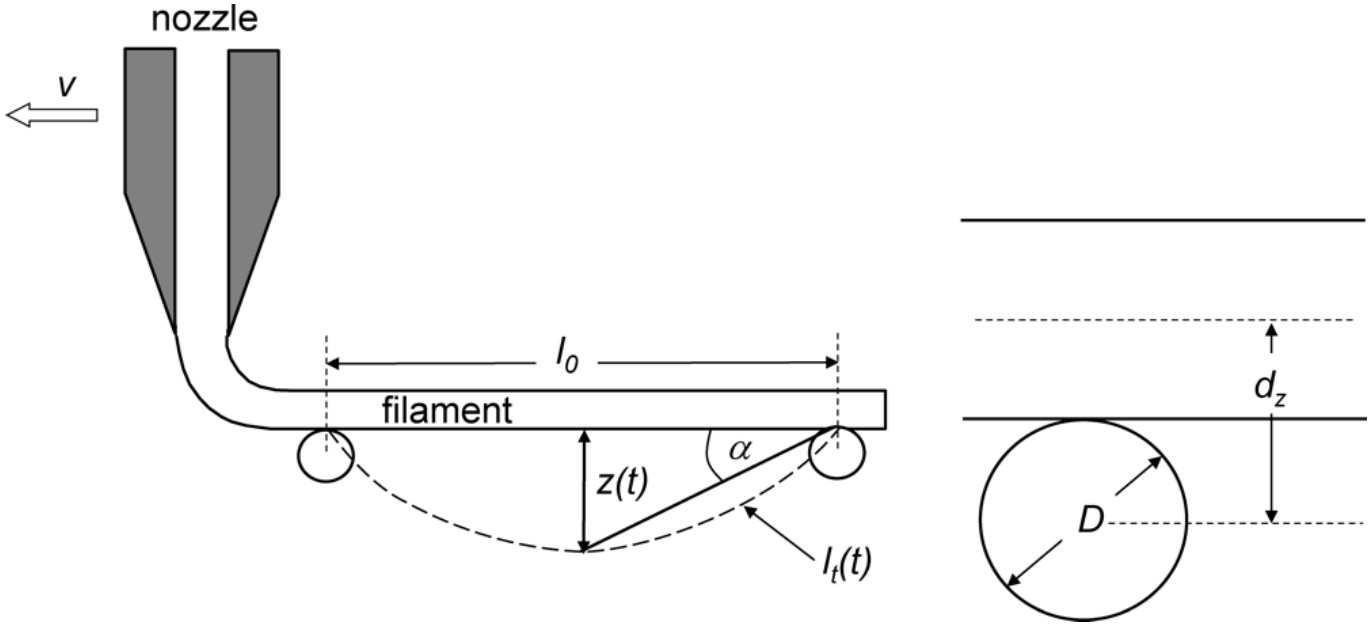

Fig. 5: Geometrical parameters applied for calculation of midspan deflection of spanning ligaments.

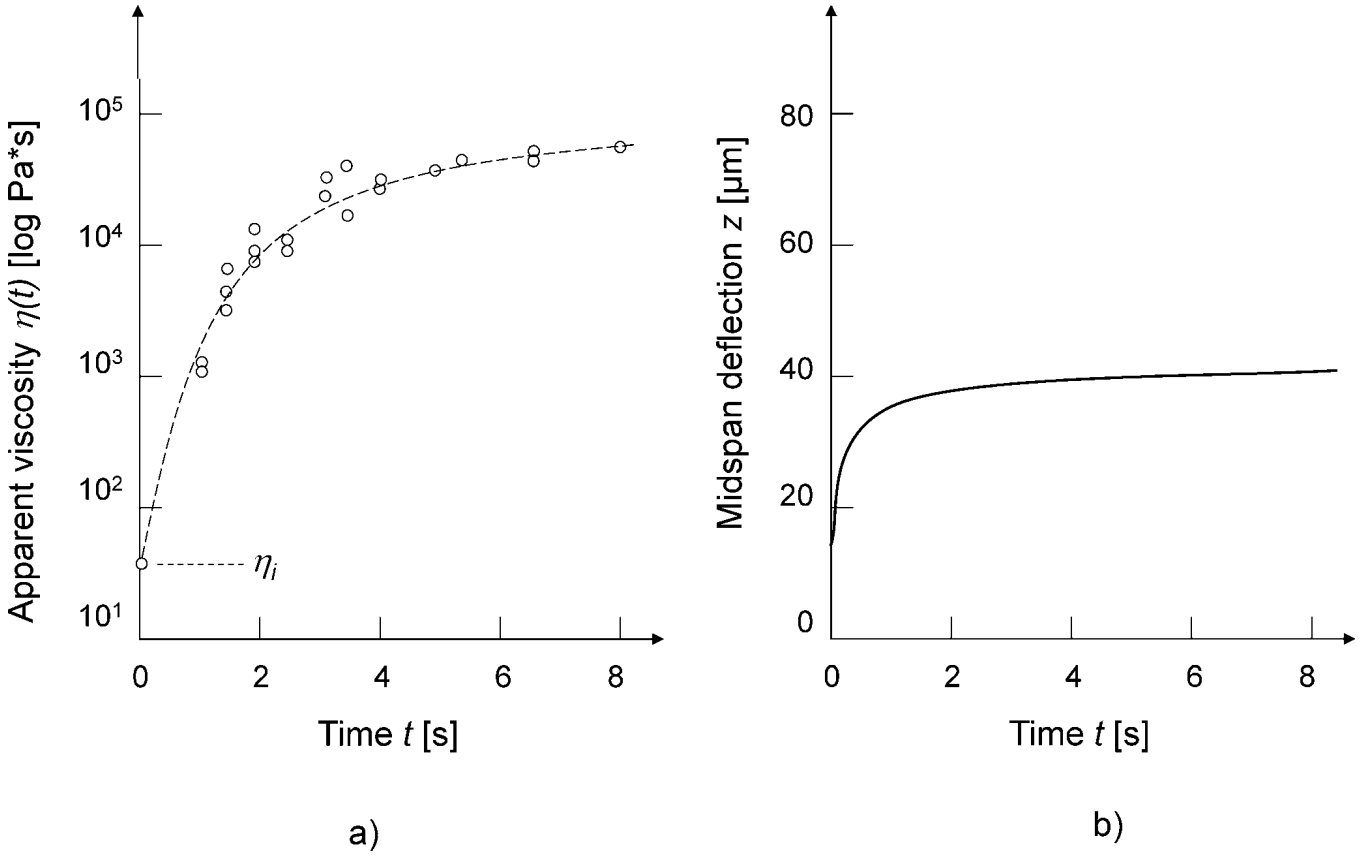

Fig. 6: a) Recovery of viscosity (τ = 100 Pa, preshear dγ/d = 100 s^{-1}) of colloidal alumina gel coagulated with 30 g/l NH_4Ac; b) calculated midspan deflection over time (filament thickness 500 µm, unsupported beam length 1000 µm).

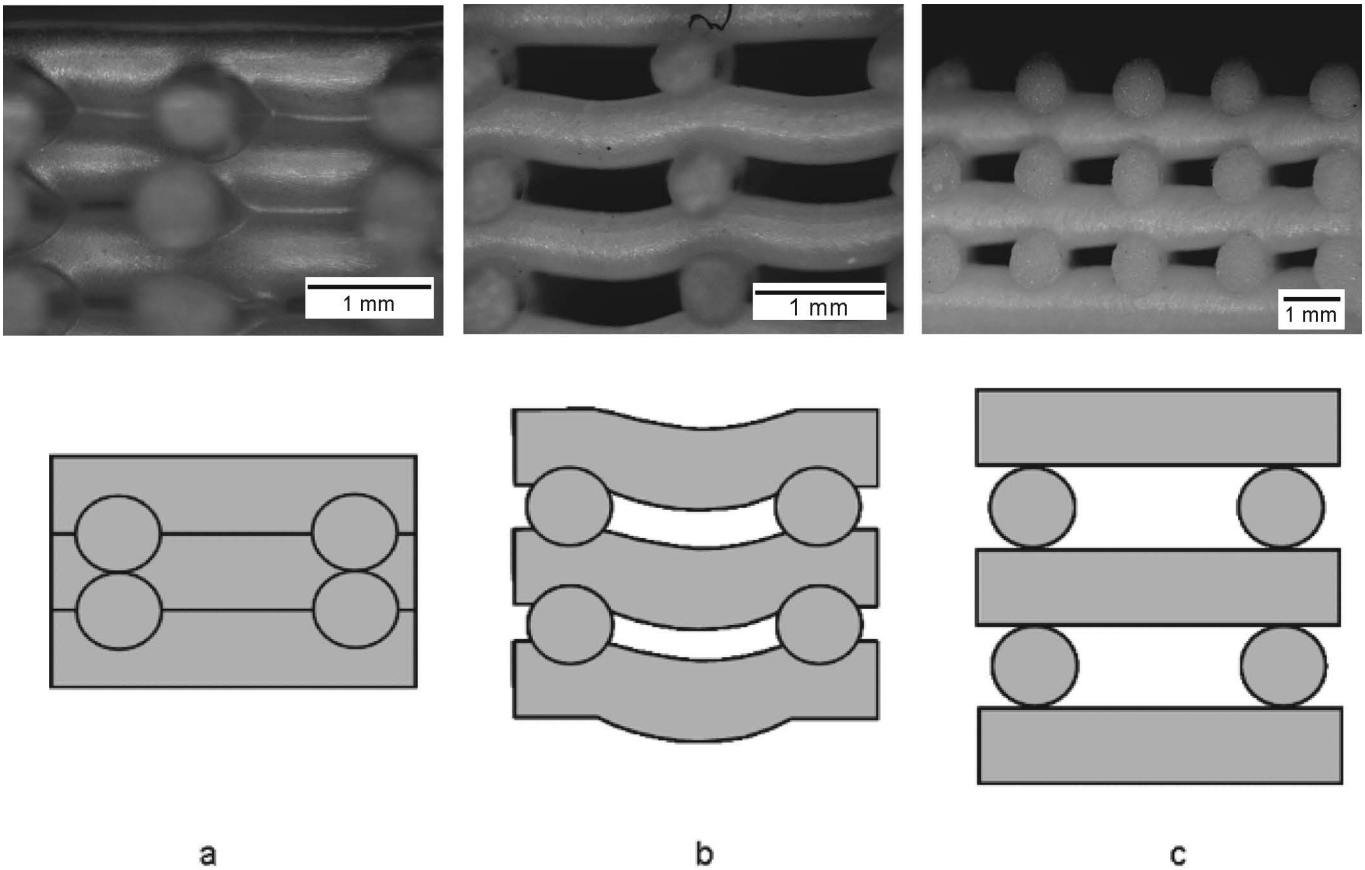

Fig. 7: Wall structures of sintered alumina lattice truss structures perpendicular to the deposition plane of robocasting applying a constant deposition rate of 35 mm/s: a) sealed walls ($d_z = D/2$; 30 g/l NH_4Ac); b) meshed walls with spanning but deflected ligaments ($d_z = D$, 30 g/l NH_4Ac); c) meshed walls with almost undeflected ligaments ($d_z = D$, 50 g/l NH_4Ac).

IV. Conclusions

Three-dimensional alumina lattice truss structures were fabricated by means of extrusion with a high-precision robotic system. An aqueous alumina-loaded gel coagulated with ammonium-acetate provided adequate rheological properties to produce periodical three-dimensional meshes with excellent shape stability after deposition and sintering. Conditions for shape evolution to attain unsupported spanning structures under the constraints of the robocasting process were discussed. Replacing circular-shaped extrusion nozzle geometry to deposit non-circular and hollow filament shapes offers a high potential of the robot-controlled filament deposition process for fabrication of lightweight lattice truss structures with versatile pore structures and component size and shape.

Acknowledgements

The authors thank the Deutsche Forschungsgemeinschaft (DFG-Koselleck GR 961/32) and the Cluster of Excellence "*Engineering of Advanced Materials*" for providing financial support. The Institute for Polymer Materials at the University of Erlangen-Nuernberg is acknowledged for the rheological measurements.

References

1 Lewis, J.A., Smay, J.E., Stuecker, J., Cesarano III, J.: Direct ink writing of three-dimensional ceramic structures (feature), *J. Am. Ceram. Soc.*, **89**, 3599 – 609, (2006).

2 Cesarano III, J., Segalman, R., Calvert, P.: Robocasting provides moldless fabrication from slurry deposition, *Ceram. Ind.*, **148**, 94 – 102, (1998).

3 Lewis, J.A.: Direct ink writing of 3D functional materials, *Adv. Funct. Mater.*, **16**, 2193 – 204, (2006).

4 Smay, J.E., Cesarano III, J., Lewis, J.A.: Colloidal inks for directed assembly of 3-D periodic structures, *Langmuir*, **18**, 5429 – 37, (2002).

5 Morissette, S.L., Lewis, J.A., Cesarano III, J., Dimos, D.B., Baer, T.: Solid freeform fabrication of aqueous alumina-poly(vinyl alcohol) gelcasting suspensions, *J. Am. Ceram. Soc.*, **83**, 2409 – 16, (2000).

6 San Marchi, C., Kouzeli, M., Rao, R., Lewis, J.A., Dunand, D.C.: Alumina-aluminum interpenetrating phase composites with three-dimensional periodic structure, *Scr. Mater.*, **49**, 861 – 6, (2003).

7 Mason, M.S., Huang, T., Landers, R.G., Leu, M.C., Hilmas, G.E.: Aqueous-based extrusion of high-solids loading ceramic pastes: process modeling and control, *J. Mater. Proc. Tech.*, **209**, 2946 – 57, (2009).

8 Stuecker, J.N., Cesarano III, J., Hirschfeld, D.A.: Control of the viscous behavior of highly concentrated mullite suspensions for robocasting, *J. Mater.Proc. Tech.*, **142**, 318 – 25, (2003).

9 Smay, J. E., Cesarano III, J., Tuttle, B.A., Lewis, J.A.: Directed colloidal assembly of linear and annular lead zirconate titanate arrays, *J. Am. Ceram. Soc.*, **87**, 293 – 5, (2004).

10 Miranda, P., Saiz, E., Gryn, K., Tomsia, A.P.: Sintering and robocasting of β-tricalcium phosphate scaffolds for orthopaedic applications, *Acta Biomater.*, **2**, 457 – 66, (2006).

11 Saiz, E., Gremillard, L., Menedez, G., Miranda, P., Gryn, K., Tomsia, A. P.: Preparation of porous hydroxyapatite scaffolds, *Mater. Sci. Eng.*, **27**, 546 – 50, (2007).

12 Şakar-Deliormanli, A., Çelik, E., Polat, M.: Rheological behavior of PMN gels for solid freeform fabrication, *Colloids Surf. A*, **324**, 159 – 66, (2008).

13 Wang, J., Shaw, L.L.: Rheological and extrusion behavior of dental porcelain slurries for rapid prototyping applications, *Mater. Sci. Eng. A*, **397**, 3314 – 21, (2005).

14 Nadkarni, S.S., Smay, J.E.: Concentrated barium titanate colloidal gels prepared by bridging flocculation for use in solid freeform fabrication, *J. Am. Ceram. Soc.*, **89**, 96 – 103, (2006).

15 Kiratzis, N., Faers, M., Luckham, P.F.: Depletion flocculation of particulate systems induced by hydroxyethylcellulose, *Colloids Surf. A*, **151**, 461 – 71, (1999).

16 Nickerson, C.S., Kornfield, J.A.: A "cleat" geometry for suppressing wall slip, *J. Rheol.*, **49**, 865 – 74, (2005).

17 Roberts, M.T., Mohraz, A., Christensen, K.T., Lewis, J.A.: Direct flow visualization of colloidal gels in microfluidic channels, *Langmuir*, **23**, 8726 – 31, (2007).

18 Krieger, I. M.: Rheology of monodisperse lattices, *Adv. Colloid. Interf. Sci.*, **3**: 111 – 36, (1972).

19 Choi, G.N., Krieger, I.M.: Rheological studies on sterically stabilized model dispersions of uniform colloidal spheres: II. steady-shear viscosity, *Adv. Colloid. Interf. Sci.*, **113**, 101 – 13, (1986).

20 Lewis, J. A.: Colloidal processing of ceramics, *J. Am. Ceram. Soc.*, **83**, 2341 – 59, (2000).

21 Greener, J., Evans, J.R.G.: Uniaxial elongational flow of particle-filled polymer melts, *J. Rheol.*, **42**, 697 – 710, (1998).

22 Buscall, R., McGowan, J.I., Morton-Jones, A.J.: The rheology of concentrated dispersions of weakly attracting colloidal particles with and without wall slip, *J. Rheol.*, **37**, 621 – 41, (1993).

23 Herschel, W.H., Bulkley, R.: Consistency measurements of rubber-benzene solutions (in german), *Kolloid Z.*, **39**, 291 – 300, (1926).